ISSN: 0974-5823 Vol. 7 No. 2 February, 2022

International Journal of Mechanical Engineering

Effect of gravity on Non-Linear Modeling and Stability of a Pneumatic Levitation System

[1,2]Moreano, G.

[2]Cajamarca, julio

[3]J. Hernández,

[4]E. Villcrés, S.

[1,2,3,4]University Professors. Escuela Superior Politécnica de Chimborazo. Facultad de Mecánica. Riobamba – Ecuador.

[1]PhD student. Pontifica Universidad Catolica del Perú. Lima – Perú.

ABSTRACT

Pneumatic applications are currently focused on industrial force processes such as pistons and levers, but this resource can be used to generate other types of applications such as automatic transport of objects with high precision through the application of control techniques on the position of the mentioned objects, the present work shows a proposal of non-linear dynamic modeling of a pneumatic levitator with a different approach to previous works, considering the gravitational force as a constant input of the system.In common mechanical systems the gravitational force is omitted when considering part of elastic systems, in this case the object to levitate does not have an elastic component so it is essential to consider gravity and its effect on the position of the object obtained from the non-linear model, its output was checked before different stimuli and it was compared with a response curve of a real model, the results were suitable since the responses were very similar, in addition an attempt to linearize the two-input mode was madel in order to study its stability and controllability and identify a suitable linear or non-linear regulator in subsequent lines of work without the need for a physical model.

Keywords: [**N**onlinear modeling], [**C**ontrollability], [**S**tability], [**G**ravitational force], [[**P**neumatic levitation]].

Introduction

Pneumatic systems are very common in industrial processes, whereupon, air pressure is used to push pistons or rotate dividing plates by opening or closing bypass valves that are generally ON-OFF control valves, that is, they allow or not air flow; Recently, with the evolution of control systems and micro-processed devices, several study options have appeared for the development of pneumatic systems that involve continuous control trends to allow the regulation of physical parameters such as the position or speed of movement of certain objects.

The main applications of these pneumatic control systems are mainly focused on improving the precision with which certain industrial processes are carried out, for example, regulating the output position of a pneumatic piston to obtain greater precision when moving or pushing objects; several examples can be seen in (Caldas et al., 2012; van Varseveld & Bone, 1997), the main drawback when working with a fluid such as air is that its turbulent behavior turns its dynamics into a nonlinear system, which generates several difficulties when trying to control its operation, due to this, in the last 10 years it has been tried to find a suitable regulator for this type of system, for example in (Shih & Ma, 1998) a fuzzy control technique is presented by applying a PWM signal to a solenoid valve, or in (Korondi & Gyeviki, 2006) the authors present a non-linear model of the pneumatic cylinder and a robust control by sliding modes that aims to maintain the stability of the cylinder at high load values, other works such as (Medrano-Cerda et al., 1995; Rao & Bone, 2008) show the application of non-linear controls to pneumatic cylinders such as adaptive control, (Bone & Ning, 2007) were the authors that show an efficiency comparison of different nonlinear control techniques for these pneumatic systems.

Another type of application of the controllability of pneumatic systems is the application in robotics where the speed and position of a piston must be controlled with great precision, for example, in parallel robots such as the Da Vinci medical robot, in (Escano et al., 2005) a complete study of the implementation of pneumatic piston speed control in a parallel robot and the effect on its kinematic and dynamic model is shown.

The study and use of pneumatic systems for the movement of objects solely by air pressure takes just under 5 years, which is why the bibliography on the subject is quite limited but it is true that in this time it has become popular. the manufacture of prototypes of levitation with didactic purposes, in (Escano et al., 2005) One of the first documented studies related to pneumatic levitation is presented, applying different control techniques on a transfer function model, a complete analysis of the physical behavior of an object levitating by the action of an air pressure is presented in (Li et al., 2008a) and a dynamic analysis of the movement is shown in (Li et al., 2008b). Other works such as the one presented in (Chaos et al., 2020) o (Chacon et al., 2017) show the construction of experimental prototypes of levitation for the application of different control systems.

At present, pneumatic levitation systems have taken interest among researchers for new applications such as the transport of objects and people, for instance pneumatic elevators that eliminate the dependence on thick cables and expensive weights for their operation or the innovative idea of the visionary Elon Musk "Drexel" who seeks to transport people between two cities by means of low pressure and high aerodynamic pipelines, another example can be seen in (Fukuta et al., 2003), These examples show the interest in this type of system due to its low costs and speed of operation.

Most of the works cited above have the weakness that the mathematical models that were used are linear, they were obtained without considering the effect of the gravitational force, a situation that greatly affects the tuning of controllers, thereby forcing them to be finely regulated. Experimentally or empirically, this work presents a non-linear modeling proposal for the pneumatic levitation system where the entire system is modeled considering the effect of the turbulent fluid and the gravitational attraction force.

Modeling

The pneumatic levator is composed of a limited number of elements, they are shown in Figure 1, the main operating element is the permanent magnet direct current motor coupled to a turbine that will generate the air flow, the second important element is the duct through which the fluid will circulate and finally the object to levitate (expanded polystyrene sphere) is the third element under consideration for obtaining the dynamic model.

Due to the operation of the system it is easy to realize that electrical, mechanical and fluid movement systems are involved; the modeling of the system begins considering its mechanical behavior, Figure 1 shows the forces that perform work on the sphere when it is levitating.

Where mg is the action of gravity (weight), F_B is the thrust force that will lift the sphere and F_{RA} is the aerodynamic resistance force that opposes the movement of the sphere, in Figure 1 this force has been presented as a shock absorber simply to represent it as a force that opposes the movement, but it must be specified that the model to be obtained will be non-linear, so that in the analysis all the variables of an aerodynamic drag force will be considered. The resistance force will always be opposite to the movement of the sphere, whether it is ascending or descending.

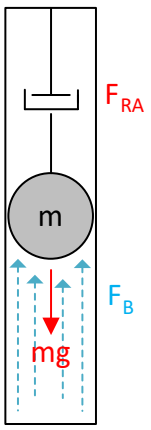

Figure 1. Free-body diagram of the sphere

Source : Authors

The modeling of the mechanical component of the system can be obtained through Newton's second law or through Euler-Lagrange modeling, both analyzes will result in equation 1.

$$my'' = F_B - F_{RA} - mg \qquad (1)$$

The thrust force $\boldsymbol{F_B}$ is directly proportional to the pressure generated by the air over the area of the sphere, that is:

$$F_B = PA \qquad (2)$$

Where P is the air pressure generated by the turbine and A is the area of the sphere that will be in direct contact with the air pressure. According to **(Orozco & Bedoya Loaiza, 2007)** the air pressure produced by a fan or turbine can be obtained as:

$$P = \frac{\delta {v_A}^2}{2} \qquad (3)$$

Where δ is the density of the fluid in motion in this case air ($\delta = 1.29\ kg/m^3$), $v_A$is the speed of the air and g the speed of the acceleration ($9.81\ m/s^2$). In turn, the speed of the air expelled by the fan is determined by the equation:

$$v_A = \frac{Q}{A_d} \tag{4}$$

Q represents the circulating air flow and A_d is the area of the duct. Knowing that the air flows at a given angular speed of the turbine, the flow at any speed can be known through the relation of equation 5.

$$Q = Q_N \left(\frac{\omega}{\omega_N}\right) \tag{5}$$

Where Q_N is a known air flow at an angular speed ω_N (which is the nominal speed of the motor) and ω is the angular speed of the fan at a given instant. Combining equations 2 to 5 the following relationship can be obtained:

$$F_B = \frac{\delta {Q_N}^2 A}{2g{A_d}^2{\omega_N}^2}\omega^2 \tag{6}$$

Equation 6 shows that the thrust force is directly proportional to the square of the angular velocity of the turbine, all the terms other than ω are constants that can be determined from the real physical model, so from now on it will be replaced by an arbitrary constant C.

The aerodynamic drag force for fluids is obtained from the relationship shown in equation 7.

$$F_{RA} = \frac{1}{2} C_d \delta A v^2 \tag{7}$$

Where A is the cross-sectional area of the moving object (in this case the sphere), v is the speed of the object, thus, y', δ is the density of the fluid that generates the resistance and C_d is the drag coefficient . Since it is a turbulent flow, equation 7 would not be valid one hundred percent, but it generates an approximation that will be used in this case to simplify the complexity of the model. The drag coefficient C_d is the most difficult value to determine from equation 8 and has to do with the Reynolds number for laminar and turbulent fluids, see (Sarpkaya, 1966; Weygand et al., 2007), a coefficient that can be determined with equation 8.

$$Re = \frac{\delta l v}{\eta} \tag{8}$$

Where l is the length of the cross section of the moving object and η represents the dynamic viscosity of the opposing fluid ($\eta\_aire\ = \ 18.2x10^{-6}\ Pa \cdot s$), this expression is frequently cited in fluid mechanics references and you can also find the expression shown in equation 9 to determine the drag coefficient as a function of the Reynolds number.

$$Cd \approx \frac{24}{Re} + \frac{6}{1+\sqrt{Re}} + 0.4 \tag{9}$$

For laminar fluids, the second and third terms of equation 9 can be neglected and combining them with equation 8 and the cross-sectional area of the sphere, the expression of the aerodynamic drag force is reduced to:

$$F_{RA} = 0.4\pi\delta r^2 v^2 \tag{10}$$

Equation 11 shows that, for movements at low speeds, the drag force is directly proportional to the square of the speed of movement, Since the motion of the sphere is not that fast, a more exact approximation of the drag force is not needed, the constant values in equation 11 will be simplified by an arbitrary constant B.

The equation that relates the voltage applied to the turbine motor with its angular velocity would complete the system model, being a direct current motor with permanent magnets, it is known to have a series configuration as shown in Figure 2, where R_a and L_a are the armature resistance and inductance respectively, V is the voltage applied to the motor terminals, i_a is the current absorbed by the motor, and E_a is the counter-electromotive force generated by the motor.

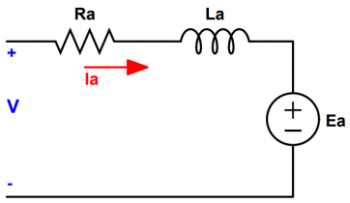

Figure 2. Equivalent circuit of a DC motor

Source : Authors

DC motors are very common actuators in control systems and their mathematical modeling is more than established in the current literature as we can see in (Antolines, 2020; Cuero Ortega, 2018; Sebastian & Alvarado, 2012). Equation 11 show two well-known expressions for DC motors that represent the generated torque and the back electromotive force as a function of the magnetic flux, the angular velocity and a machine construction constant k.

$$\tau(t) = K_T(t)\phi i_a(t)$$
$$E_a(t) = K_v(t)\phi\omega(t) \qquad (11)$$

Regularly the constant K_T that influences the torque has a numerical value identical to the constant K_v that influences the back electromotive force despite the fact that they represent different characteristics of the motor; the combination of the constants and the magnetic flux ϕ are associated into a single constant k for the DC motor model. Meanwhile the electric model of the motor has the following form:

$$v(t) = R_a i_a(t) + L_a \frac{di_a(t)}{dt} + E_a \qquad (12)$$

For the mechanical behavior of the motor, the system shown in Figure 3 is considered.

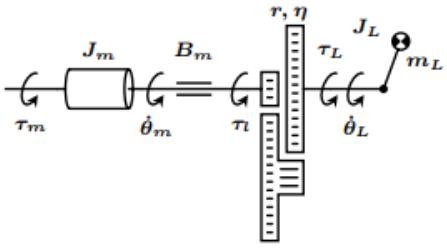

Figure 3. Rotational movement of DC motor

Source : (Monasterio & Gutierrez, 2020)

Equation 13 represents the summation of moments about the axis of rotation of the motor, where I is the moment of inertia of the motor about its axis of rotation, M_L is the moment of opposition that produces the load and M_f is the moment of viscous friction.

$$I\alpha = \tau(t) - M_f - M_L \quad (13)$$

By ordering the terms and coupling to the known variables, equation 13 can be rewritten as:

$$I\omega' = \tau(t) - B_m\omega - M_L \quad (14)$$

Where B_m is the viscous friction constant of the motor, according to (Elizabeth et al., 2019) manufacturers rarely give the value of the viscous friction coefficient, but they do provide other parameters that allow obtaining its value, two forms are indicated which are shown in the equations 15 and 17.

$$B_m = \frac{I}{t_m} - \frac{k_T k_v}{R_a} \quad (15)$$

Where t_m is the mechanical time constant, it is so called because it is obtained by eliminating the electrical coupling in the motor equations, that is, neglecting what is called the electrical time constant $(t_e = L_a/R_a)$, for this it is assumed $L_a = 0$.

$$t_m = \frac{R_a I}{R_a B_m + k_T k_v} \quad (16)$$

Note that the mechanical time constant is a function of the viscous friction constant, which is why this equation would not be useful for the required objective, the second way to determine the constant is to use the maximum no-load motor current I_o the nominal speed motor ω_N as shown in equation 17.

$$B_m = \frac{k_T I_o}{\omega_N} \quad (17)$$

Additionally, in (Monasterio & Gutierrez, 2020) an experimental method is presented to obtain the viscous friction constant in case none of the parameters of the motor to be used in the turbine are known, in this work the value of the constant and will be verified experimentally to verify the percentage of reliability that the approximation of equation 17 presents.

With these considerations, the equations that describe the movement of the sphere within the ventilation duct are equations 1, 12 and 14 and can be expressed as follows:

$$i_a' = \frac{1}{L_a}v - \frac{R_a}{L_a}i_a - \frac{K}{L_a}\omega$$

$$\omega' = \frac{K}{I}i_a - \frac{B_m}{I}\omega \quad (18)$$

$$y'' = \frac{C}{m}\omega^2 - \frac{B}{m}y'^2 - g$$

Real system Model

In this section, physical parameters and equations will be obtained in order to be able to simulate the system.There are values that are easier to obtain, such as the mass of the sphere, and other more complicated ones, as seen in the previous section. Table 1 shows known constants and other values that are easy to obtain analytically.

Table 1. Actual system parameters

Parameter	Value
m	$0.002\ Kg$
δ	$1.29\ Kg/m^3$
g	$9.81\ m/s^2$
A_d	$2.55x10^{-3}\ m^2$
A	$0.01\ m^2$
B	$9.77x10^{-6}\ Kg/s$

Source : Authors

Regarding the movement of the air, the only value that cannot be gotten analytically is the nominal flow Q_N, so its value was obtained experimentally by measuring the pressure generated by the fluid on the end of the pipeline and replacing its value in equations 3 and 4.

Table 2 shows known values from the manufacturer of the motor used in the built model turbine, in addition, simple values to obtain such as resistance and inductance are indicated.

Table 2. Actual DC motor parameters

Parameter	Value
ω_N	$13000\ RPM$
V_N	$9\ V$
R_a	$5.8\ \Omega$
L_a	$1\ mH$

Source : Authors

Determination of the speed constant (k_v): The speed constant k_v directly relates the back electromotive force of the motor with its angular velocity when the magnetic flux is constant (it is always true for a permanent magnet motor). Its value can be determined experimentally, measuring current values in the armature and determining the back electromotive force for different operating speed conditions. Once this process was carried out, the data shown in Table 3 were obtained and presented with red asterisks in Figure 4, additionally different values of k_v were obtained by applying equation 1.

Table 3. k_v values obtained experimentally

$E_a\ (V)$	$\omega\ (rad/s)$	$k_v\ (Vs/rad)$
0,56	240.8	0.0023
1,13	394.1	0.0029
1,78	596.8	0.003
2,38	795.7	0.003
2,80	916.1	0.0031
3,39	1005.1	0.0034
3,87	1225	0.0032
4,29	1308.8	0.0033
5,23	1361.1	0.0038

Source : Authors

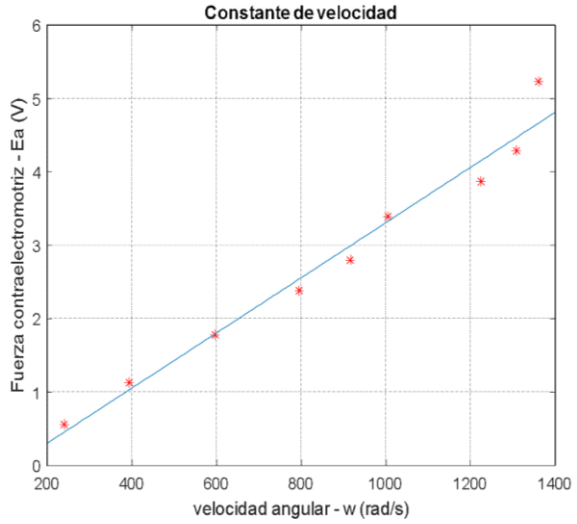

Figure 4. k_v values and their linear approximation

Source : Authors

Figure 4 shows that not all the values obtained experimentally have a linear relationship, so an approximation by least squares is carried out to know the slope of the line that best relates all the points obtained, the equation of the line is shown in the equation 24. The constant k_v can then be determined as:

$$k_v = 0.0038\ \frac{Vs}{rad} \qquad (19)$$

The torque constant k_T and the speed constant k_v are numerically identical in the international measurement system.

Determination of the mechanical constant (t_m): The mechanical constant of a motor directly relates the excitation voltage to the motor speed, this constant can be determined by applying a transient voltage signal to the motor from a minimum value to the nominal operating value, the constant that relates the speed change of the motor with the voltage step is known as the mechanical constant, this experimentation is achieved with the help of an oscilloscope by freezing the voltage transition with respect to time, as seen in Figure 5.

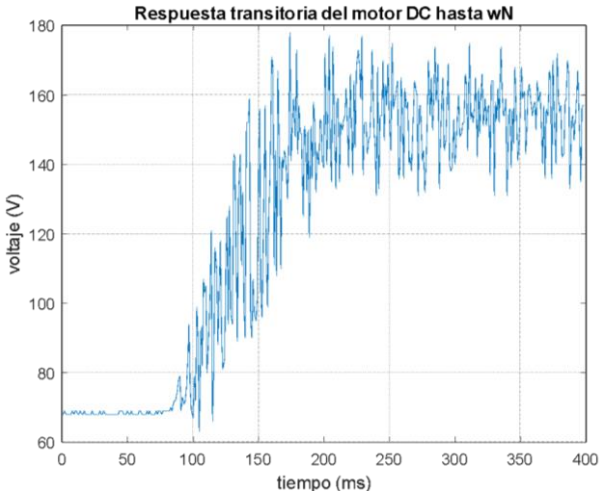

Figure 5. Transient response of the DC motor up to its rated speed

Source : Authors

Although the noise generated in the signal due to the chipping of the brushes is quite high, the transient curve that is desired for the experimental procedure can be appreciated. The mechanical time constant coincides with the time it takes for the crow to reach 63.2% of its maximum value, in this case:

$$t_m = 180\ ms \qquad (20)$$

Determination of the motor viscous friction constant ($\boldsymbol{B_m}$): The viscous friction constant can be obtained analytically with the nominal current of the no-load motor ($\boldsymbol{I_o = 0.65\ A}$) and its value applied in equation 17, resulting:

$$B_m = 1.73x10^{-6}\ Nm \cdot s \qquad (21)$$

To determine how efficient the analytically found value is, a second value of $\boldsymbol{B_m}$ will be obtained experimentally, from equation 11 it is known that the torque of the motor is proportional to the current it absorbs and by equating this value with equation 14 it is obtained :

$$\tau = k_T I_a = I\omega' + B_m\omega \qquad (22)$$

The constant $\boldsymbol{B_m}$ is determined when the motor is running under stable conditions, that is, when the angular acceleration is zero, from equation 22 it is observed that $\boldsymbol{B_m}$ directly relates the motor torque with the angular velocity, so values can be obtained experimental as shown in Table 4.

Table 4. Torque vs angular velocity

$V\ (V)$	$I_a\ (A)$	$\tau = k_T I_a\ (Nm$	$\omega\ (rad/s)$
1.2	0,11	0,0003	240.8
2	0,15	0,0004	394.1
3	0,21	0,0006	596.8
4	0,28	0,0008	795.7
5	0,38	0,0012	916.1
6	0,45	0,0015	1005.1
7	0,54	0,0017	1225
8	0,64	0,0021	1308.8
9	0,65	0,0025	1361.1

Source : Authors

Figure 6 shows the points obtained from the mechanical torque versus the angular velocity of the motor and again by means of a least squares approximation the line that best relates all these points can be obtained.

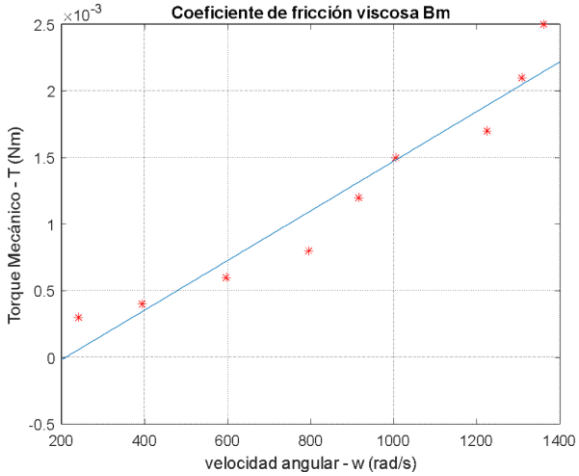

Figure 6. Torque vs angular velocity

Source : Authors

When comparing the values of equations 21 and 23, it is observed that the error between the analytical and experimental method is extremely small, so either of the two values would be acceptable for the implementation of the model.

$$B_m = 1.9x10^{-6}\ Nm \cdot s \qquad (23)$$

*Determination of the moment of inertia of the motor (**I**):* Knowing the viscous friction constant and the mechanical time constant, it is easy to obtain the value of the inertia of the motor analytically through equation 16, it results:

$$I = \frac{t_m(R_a B_m + k_T k_v)}{R_a} = 7.9x10^{-7}\ Kgm^2 \qquad (24)$$

Real model equations: Once the experimental tests have been carried out and certain analytical values have been obtained, the equations of motion of the levitator result:

$$i_a' = 1000v - 5800i_a - 3.8\omega$$

$$\omega' = 4810.12i_a - 2.3\omega \qquad (25)$$

$$y'' = 4.12x10^{-5}\omega^2 - 11.2295\, y'^2 - g$$

Linearization

Since the model obtained incorporates a non-linear equation to analyze its stability and controllability in a simpler way, it is advisable to linearize said equation around an equilibrium point, this equilibrium point will be when $\boldsymbol{y' = 0}$ and $\boldsymbol{y'' = 0}$, that is, when the sphere is not in motion. The equation linearized through a Taylor series around the equilibrium point is of the general form:

$$y'' - \underline{y''} = a(\omega - \underline{\omega}) + b(y' - \underline{y'}) - g \qquad (26)$$

Where:

$$a = \frac{\delta f(\omega, y')}{\delta \omega}$$

$$b = \frac{\delta f(\omega, y')}{\delta y'} \qquad (27)$$

If each constant in equation 27 is evaluated for $\boldsymbol{\omega = \underline{\omega}}$ and $\boldsymbol{y = \underline{y'}}$ the linear equation is obtained:

$$y'' = 0.0346\omega - 11.2295y' - 24.34 \qquad (28)$$

If the following state variables are set: $\boldsymbol{x_1 = i_a, x_2 = \omega, x_3 = y}$ **y** $\boldsymbol{x_4 = y'}$, the linear system is modeled as:

$$A = \begin{bmatrix} -\frac{R_a}{L_a} & -\frac{k}{L_a} & \frac{k}{I} \\ -\frac{B_m}{I} & 0 & 0 \\ 0 & 0 & 0 \\ 0 & 0 & 0 \\ 0 & 0.0346 & -11.22 \end{bmatrix} \qquad (29)$$

$$B = [1/L_a\ 0\ 0\ 0 \quad 0\ 0\ 0\ -15.126\ ]$$

$$C = [0\ 0\ 1\ 0\ ] \quad \text{y} \quad D = [0\ 0\ ]$$

At this point it is important to mention that the effect of gravity plus the factors that have been added as a result of the linearization of the system are associated as an input to the system, unlike certain mechanical models where the factor of gravity is integrated to the constant of a spring, in this case, gravity acts directly on the moving sphere, that is, the linear model is represented as a system of two inputs and one output.

The transfer function representation of the system will be composed of a matrix of transfer functions as seen in equation 30.

$$Y(s) = \left[\frac{166430}{s^4 + 5810s^3 + 96770s^2 + 354990s} \quad \frac{-20s}{s^4 + 5810}\right. \quad (30)$$

Model comparison

To verify the similarity of the mathematical models, a series of experimental data were obtained from a real prototype in which two types of control signals were entered, the first represents a test pulse in within the sphere rises when the angular velocity has a value slightly higher than the equilibrium value and the second signal showing different control values (see Figure 7).

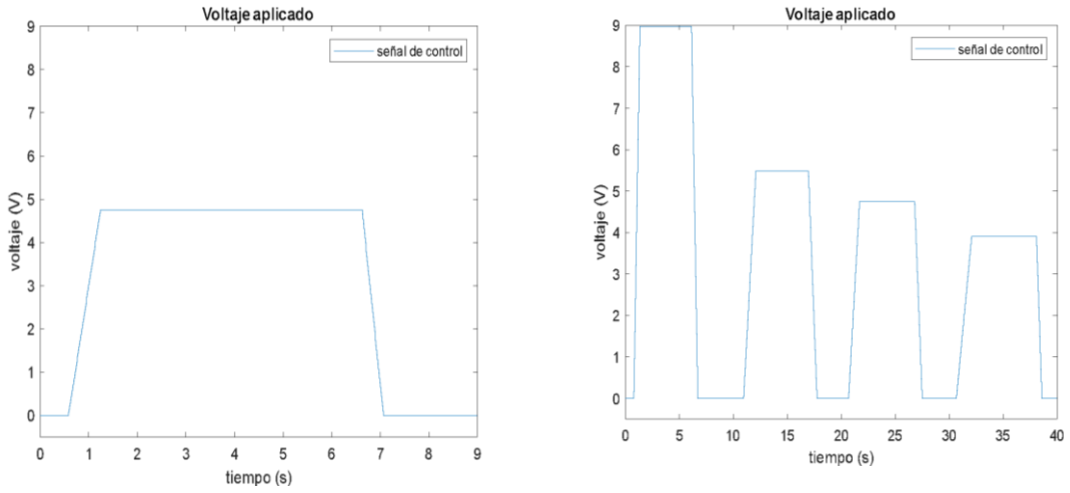

a) b)

Figure 7. Figura X. Señales de control para prueba de los modelos matemáticos. a) Pulso único. b) Tren de pulsos de varios valores de operación.

Source : Authors

Figure 8 shows the non-linear model built in Simulink used to evaluate the displacement of the sphere within the real limits of the prototype, for its part the linearized model was simulated using the proper block of state space, in addition a linear model using the Matlab system identifier to evaluate its efficiency in this type of system.

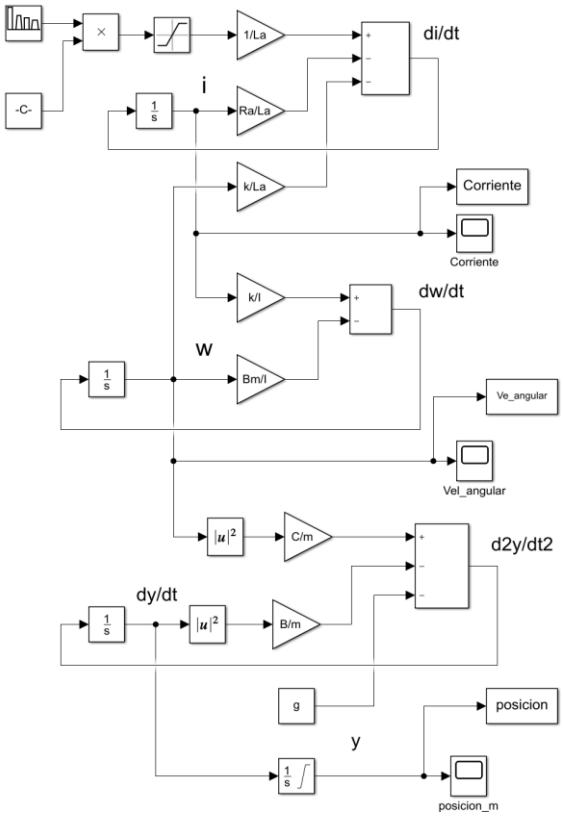

Figure 8. Nonlinear model in Simulink

Source : Authors

Figure 9 shows the response curve of the prototype, the non-linear model, the linearized model and the model identified by Matlab to the input signal of Figure 8.a.

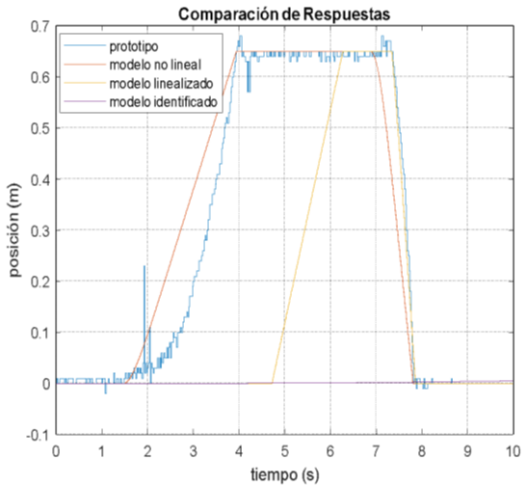

Figure 9. Responses to the pulse in Figure 8.a

Source : Authors

In Figure 9 it is easily observed that the identified linear model is the one that most closely resembles the curve of the real model, despite the fact that the rise curve is not so pronounced, the rising and falling points coincide with an extremely low error. For its part, the linearized model almost has a 100% similarity in the fall period, but at the time of rise it has a delay of at least 2 seconds, this could cause problems in certain sudden changes, but if the objective is to maintain the position of the stable sphere in the model could be used to identify certain controllers, whereas the system identified by the signal analyzer does not present a response identifying the system.

Figure 10 shows the response curves of the mathematical models obtained with the input signal shown in Figure 8.b.

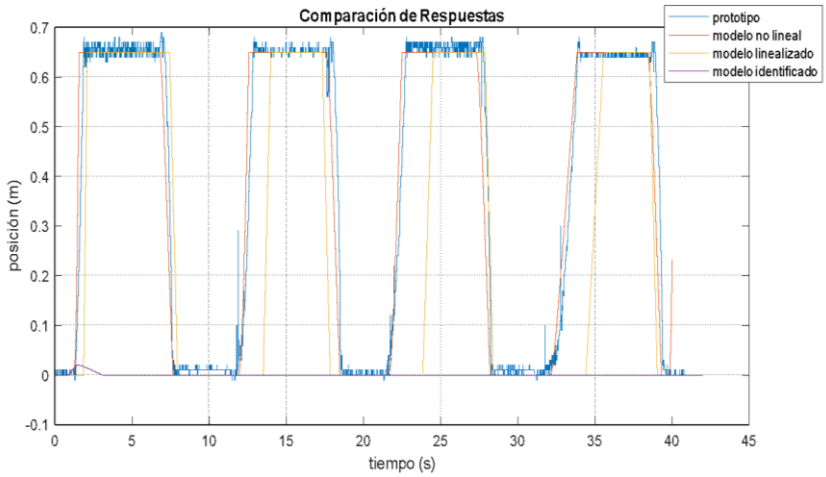

Figure 10. Response of the models to the input signal of Figure 8.b

Source : Authors

Figure 10 shows again that the previously obtained non-linear model represents the real model very precisely, the linearized model again shows the delay in the rising moments and the model identified by Matlab does not represent the system in any way.

Stability

Although the linearized model presents a certain error in the upward transitions, if the system is considered as slow, the model can be used to analyze its stability and controllability, Figure 11 shows the place of the roots of the linearized model where it is observed that There is a pole very close to the origin of the real-imaginary plane, as it is a dominant pole it means that the system is stable but very close to being oscillatory, this coincides with the experimentation where the sphere can be stabilized at any point but it is destabilized quickly in the event of minimal disturbance.

Another conclusion regarding the place of the roots is that the system will become completely unstable before any applied gain value to it since the dominant poles will move to the right half plane of the real-imaginary plane.

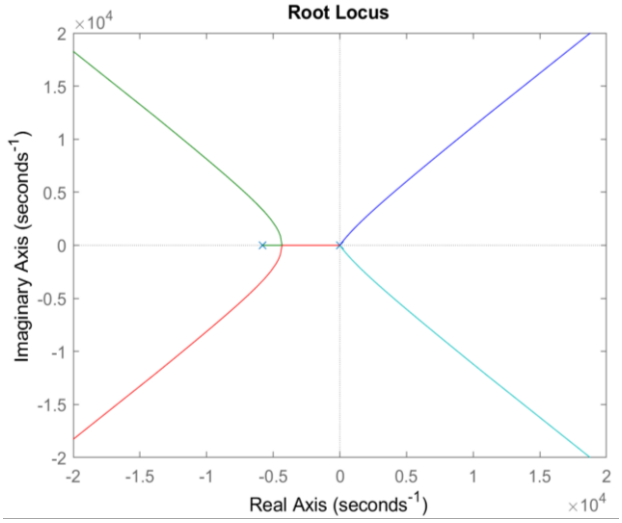

Figure 11. Root locus of the linearized model

Source : Authors

The same conclusions gotten by the root locus graph can be obtained in the frequency analysis, as seen in the Bode diagram shown in Figure 12, the profit margin and the phase margin are positive, demonstrating the stability of the system.

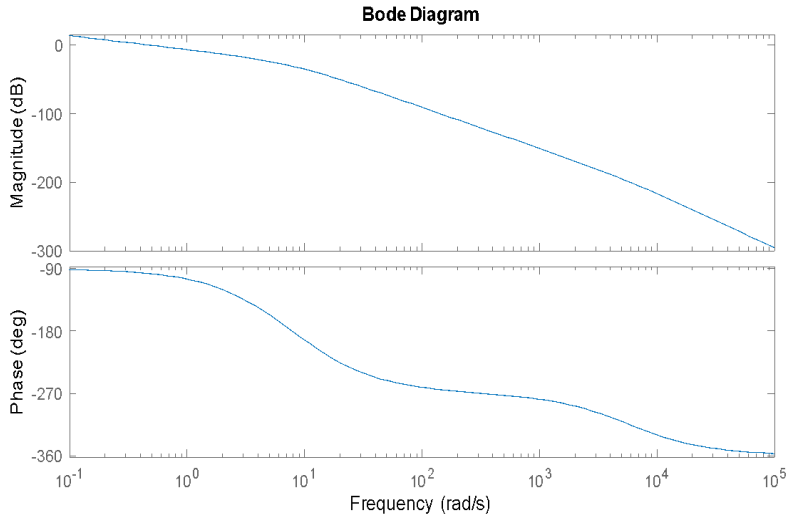

Figure 12. Bode plot of the linearized model

Source : Authors

Controllability

Finally, the controllability of the system is studied to verify that there is a linear or nonlinear regulator capable of stabilizing the system at some arbitrary operating point, for this it must be verified that no row or column of the controllability matrix has linear dependence on others. Due to the complexity of the matrix, its rank is obtained through Matlab, resulting in a rank equal to 4, this is equal to the order of matrix A, so it can be deduced that there is no linear dependence between rows and columns of the transition matrix of states.

The controllability of the system is also defined by identifying the non-singularity of the controllability matrix, one way to demonstrate is by directly obtaining matrix A in its controllable canonical form, resulting in:

$$Acc = [0 \quad 1\ 0 \quad 0\ 0 \quad 0\ 1 \\ -0.0648 \quad -3.549x10^5 \quad 0\ 1 \quad -9.67x10^4 \\ -5.81x10^3\ ] \tag{31}$$

If the matrix can be obtained in its controllable canonical form, it means that the controllability matrix is not singular, therefore the states of the system are independently linear and consequently are controllable.

Although the output is a state of the system and therefore is controllable, it can be ensured that the output of the system is controllable by verifying the range of the output controllability matrix that results:

$$Ss = [0\ 0\ 0 \quad -15.126\ 0\ 169.85 \quad 1.66x10^5 \\ -1.97x10^3\ ] \tag{32}$$

The matrix of equation 44 is the controllability matrix of the absolute output and has a rank 1 that is equal to the rank of the system output matrix C, this verifies that the output of the system that indicates the position of the sphere in the levitator is fully controllable.

Conclusions

A non-linear mathematical model of a pneumatic levator can be obtained by knowing certain characteristics of the turbine motor, the object to be levitated and the levitation duct in such a way that the real behavior of the system is reproduced almost identically, for this it is important do not forget the effect of gravity in the model since it cannot be eliminated by other components as it is done in spring mass phenomena.

The gravitational attraction force represents the main effect felt by the system when the air pressure is below an equilibrium value, this forces to include its effect on the system and since it is a constant it can be considered as an input that fixes the system trying to directly and precisely affect the state variables.

The aerodynamic drag force is one of the non-linearities of the system since its value increases when the speed of the sphere increases, in turn, a phenomenon that cannot be ruled out occurs when the movement begins since the fluid is turbulent until it is It manages to overcome the inertia of the system, when this factor is neglected when linearizing the system, there is a delay in the output response.

Finally, it is determined that the system is marginally stable since it has negative eigenvalues very close to the origin of the real-imaginary plane, this means that the system could be stabilized, but it is very sensitive to disturbances; In addition to the final analysis, it is determined that the system is fully controllable in its states and its output. In later work, different system control options will be presented.

References

1. Antolines, J. D. R. (2020). Control of a Direct Current Motor Using Time Scaling. *Ingeniería e Investigación*, *40*(3). https://doi.org/10.15446/ing.investig.v40n3.80124
2. Bone, G. M., & Ning, S. (2007). Experimental comparison of position tracking control algorithms for pneumatic cylinder actuators. *IEEE/ASME Transactions on Mechatronics*, *12*(5), 557–561. https://doi.org/10.1109/TMECH.2007.905718
3. Caldas, O., Jimenez, S., & Mejía, E. (2012). View of Identificación paramétrica en lazo cerrado de sistema de accionamiento neumático para cilindro de doble efecto. *Revista de La Facultad de Ingeniería*, 9–19. https://revistas.uptc.edu.co/index.php/ingenieria/article/view/2114/2077
4. Chacon, J., Saenz, J., Torre, L., Diaz, J., & Esquembre, F. (2017). Design of a Low-Cost Air Levitation System for Teaching Control Engineering. *Sensors*, *17*(10), 2321. https://doi.org/10.3390/s17102321
5. Chaos, D., Chacón, J., Aranda-Escolástico, E., & Dormido, S. (2020). Robust switched control of an air levitation system with minimum sensing. *ISA Transactions*, *96*, 327–336. https://doi.org/10.1016/j.isatra.2019.06.020
6. Cuero Ortega, J. D. (2018). Prototipo para modelar y controlar un motor DC. *Visión Electrónica*, *12*(1), 65–72. https://doi.org/10.14483/22484728.13754
7. Elizabeth, M., Ávila, O., Ponce, I. U., Tupak, L., Bustos, A., Israel, Á., & Marrufo, S. (2019). ESTIMACIÓN DE LOS COEFICIENTES DE INERCIA Y DE FRICCIÓN DE UN MOTOR DE CD ESTIMATION OF INERTIA AND FRICTION COEFFICIENTS OF A DC MOTOR. *Tecnológico Nacional de México En Celaya Pistas Educativas*, *41*(134). http://itcelaya.edu.mx/ojs/index.php/pistas
8. Escano, J. M., Ortega, M. G., & Rubio, F. R. (2005). Position Control of a Pneumatic Levitation System. *2005 IEEE Conference on Emerging Technologies and Factory Automation*, *1*, 523–528. https://doi.org/10.1109/ETFA.2005.1612568
9. Fukuta, Y., Mita, Y., Arai, M., & Fujita, H. (2003). Pneumatic two-dimensional conveyance system for autonomous distributed MEMS. *TRANSDUCERS 2003 - 12th International Conference on Solid-State Sensors, Actuators and Microsystems, Digest of Technical Papers*, *2*, 1019–1022. https://doi.org/10.1109/SENSOR.2003.1216941
10. Korondi, P., & Gyeviki, J. (2006). Robust Position Control for a Pneumatic Cylinder. *2006 12th International Power Electronics and Motion Control Conference*, 513–518. https://doi.org/10.1109/EPEPEMC.2006.4778451
11. Li, X., Kawashima, K., & Kagawa, T. (2008a). Analysis of vortex levitation. *Experimental Thermal and Fluid Science*, *32*(8), 1448–1454. https://doi.org/10.1016/j.expthermflusci.2008.03.010
12. Li, X., Kawashima, K., & Kagawa, T. (2008b). Dynamic characteristics of vortex levitation. *Proceedings of the SICE Annual Conference*, 1175–1180. https://doi.org/10.1109/SICE.2008.4654838
13. Medrano-Cerda, G. A., Bowler, C. J., & Caldwell, D. G. (1995). Adaptive position control of antagonistic pneumatic muscle actuators. *Proceedings 1995 IEEE/RSJ International Conference on Intelligent Robots and Systems. Human Robot Interaction and Cooperative Robots*, *1*, 378–383. https://doi.org/10.1109/IROS.1995.525824
14. Monasterio, F., & Gutierrez, A. (2020). *Modelado de un motorDC*. http://www.robolabo.etsit.upm.es/asignaturas/seco/apuntes/modelado.pdf
15. Orozco, A., & Bedoya Loaiza, F. (2007). Calculo del flujo másico y caudal de aire para un ventilador utilizado en silos para secado para del café. *Scientia et Technica Año XIII*, *35*(35). https://revistas.utp.edu.co/index.php/revistaciencia/article/view/5411
16. Rao, Z., & Bone, G. M. (2008). Nonlinear modeling and control of servo pneumatic actuators. *IEEE Transactions on Control Systems Technology*, *16*(3), 562–569. https://doi.org/10.1109/TCST.2007.912127
17. Sarpkaya, T. (1966). Experimental Determination of the Critical Reynolds Number for Pulsating Poiseuille Flow. *Journal of Basic Engineering*, *88*(3), 589–598. https://doi.org/10.1115/1.3645920
18. Sebastian, M., & Alvarado, A. (2012). Modelo matemático de un motor de corriente continua separadamente excitado: Control de velocidad por corriente de armadura. *Am. J. Phys. Educ*, *6*(1). http://www.lajpe.org

19. Shih, M. C., & Ma, M. A. (1998). Position control of a pneumatic cylinder using fuzzy PWM control method. *Mechatronics*, *8*(3), 241–253. https://doi.org/10.1016/s0957-4158(98)00005-1
20. van Varseveld, R. B., & Bone, G. M. (1997). Accurate position control of a pneumatic actuator using on/off solenoid valves. *IEEE/ASME Transactions on Mechatronics*, *2*(3), 195–204. https://doi.org/10.1109/3516.622972
21. Weygand, J. M., Matthaeus, W. H., Dasso, S., Kivelson, M. G., & Walker, R. J. (2007). Taylor scale and effective magnetic Reynolds number determination from plasma sheet and solar wind magnetic field fluctuations. *Journal of Geophysical Research: Space Physics*, *112*(A10), n/a-n/a. https://doi.org/10.1029/2007JA012486